A study on the effect of air humidity on jet flames of hydrogen ships

Huidong Jia, Zuxu An, Baiyi Qi, Guogang Yang[*], Xiangkun Ma

Marine Engineering College, Dalian Maritime University, Dalian, Liaoning, 116000, China

Abstract. With the rapid development of the shipping industry and the proposal of "double carbon" strategy, green shipping has become the center of development in China. Hydrogen-powered ships are powered by hydrogen fuel cells, which have the advantages of zero pollution, zero emission, fast charging speed, and high stability during operation; these features make hydrogen-powered ships have a broader development prospect. Due to the flammable and explosive nature of hydrogen, when hydrogen leakage occurs, combustion and explosion are very likely to occur, so hydrogen safety has also become a major problem for hydrogen-powered ships before they are widely used.In this thesis, the effect of ambient humidity on the hydrogen jet flame is investigated by numerical simulation of hydrogen jet flame generated from a hydrogen fuel cell ship in an open environment using CFD computational fluid dynamics software. The results show that under different ambient air humidity, the upper part of the jet flame is shifted to the cockpit to different degrees, and the difference of its flame shape is small. With the increase of ambient air humidity, the molar concentration of hydrogen distributed on the wall surface of the cockpit decreases gradually, and the temperature decreases gradually.

1. Introduction

Traditional fossil-fuel-powered ships mainly rely on fossil fuels such as oil and coal as their power source, and their safety problems are mainly centered on fuel leakage, fire and emission pollution. The combustion of fossil fuels produces a large amount of harmful gases and particles, which pose a threat to the environment and human health. Hydrogen-powered ships, on the other hand, use hydrogen fuel cells as their main power source, and their safety is mainly reflected in the storage and use of hydrogen. Hydrogen fuel cells themselves do not generate problems such as high temperature and high pressure, thus reducing safety risks to a certain extent.

Existing regulatory frameworks and international standards for the safety of hydrogen-powered ships include, inter alia, the Interim Guidelines for Safety in the Application of Fuel Cells to Ships, the Interim Guidelines for Safety in the Application of Hydrogen Fuel to Ships and the Interim Rules for the Technology and Inspection of Hydrogen Fuel Cell-Powered Ships. These rules will address the physical and chemical properties of hydrogen in detail. Hydrogen is a colorless, odorless, highly flammable and explosive gas with a fast diffusion rate and a wide explosive range, and these characteristics make the use of hydrogen on ships pose special safety challenges. These documents will take into account the various conditions that ships may encounter during operation, including bumps in navigation, temperature changes, humidity changes, etc., all of which may affect the safety and stability of hydrogen. Therefore, these guidelines and

rules will propose corresponding preventive measures and emergency response programs to ensure the safe use of hydrogen under these circumstances. In addition, these documents will focus on prevention and response to safety issues such as hydrogen leakage and fire. They provide for a rigorous inspection and maintenance regime to ensure the integrity of hydrogen storage equipment and systems, as well as detailed contingency plans to deal with possible hydrogen leaks or fires.

In the long term, biodiesel, hydrogen and ammonia will inevitably become the dominant alternative fuels for ships. Among them, ammonia, hydrogen and methanol are the most studied alternative marine fuels. If renewable resources are used for their production, low or zero emissions can be realized, resulting in the so-called green fuels [1].

2. Mathematical Modeling of Hydrogen Jet Flame

2.1. Governing equation

In this study, we used the steady state Reynolds average N-S system of equations (RANS) with the following control equations:

Mass conservation equations:

$$\frac{\partial}{\partial x_i}(\rho u_i) = 0 \qquad (1)$$

Momentum conservation equation:

---

[*] Corresponding author's e-mail: yanggg@dlmu.edu.cn

$$\frac{\partial}{\partial x_j}\left(\rho u_i u_j\right) = -\frac{\partial p}{\partial x_i} + \frac{\partial\left(\tau_{ij} - \rho\overline{u_i u_j}\right)}{\partial x_j} + \rho g_i \quad (2)$$

$$\tau_{ij} = \mu\left(\frac{\partial u_i}{\partial x_j} + \frac{\partial u_j}{\partial x_i} - \frac{2\partial u_k}{3\partial x_k}\delta_{ij}\right) \quad (3)$$

$$-\rho\overline{u_i u_j} = \mu_t\left(\frac{\partial u_i}{\partial x_j} + \frac{\partial u_j}{\partial x_i}\right) - \frac{2}{3}(\rho k + \mu_t\frac{\partial u_k}{\partial x_k})\delta_{ij} \quad (4)$$

Energy conservation equation:

$$\frac{\partial}{\partial t}(\rho e) + \frac{\partial}{\partial}\left(u_i\left(\rho e + p\right)\right) = \frac{\partial}{\partial x_i}\left(\left(\lambda + \frac{\mu_t c_p}{\mathrm{Pr}_t}\right)\frac{\partial T}{\partial x_i} - \sum_{m=1}^{N} h_m J_m + u_j\tau_{ij}\right) + Q_c \quad (5)$$

$$e = \sum_{m=1}^{N} Y_m h_m - \frac{p}{\rho} + \frac{1}{2}u_k u_k \quad (6)$$

Component conservation equations:

$$\frac{\partial}{\partial t}\left(\rho Y_m\right) + \frac{\partial}{\partial x_i}\left(\rho u_i Y_m\right) = -\frac{\partial J_m}{\partial x_i} + R_m \quad (7)$$

In the formula, ρ is the density, M_m is the molar mass, R_u is the universal gas constant; g is the acceleration of gravity; T is the temperature; u_i is the velocity component; p is the fluid pressure; k is the turbulent kinetic energy; μ and μ_t are the molecular viscosity and turbulent viscosity, respectively; Pr and Pr_t are the molecular Prandtl number and turbulent Prandtl number, respectively; This study takes $\mathrm{Pr} = \mathrm{Pr}_t = 0.85$; J_m diffusion flux; D_m and D_T are the mass diffusion coefficient and thermal diffusion coefficient, respectively, $Sc_t = 0.7$ is the turbulent Schmidt number; τ_{ij} is the stress tensor; $-\rho\overline{u_i u_j}$ is the Reynolds stress; δ_{ij} is the Kronecker symbol; Q_c is a source of heat released by a chemical reaction; R_m is the source term of the component conservation equation; e is the thermodynamic energy; D_m, Y_m and h_m are the diffusion coefficient, mass fraction and specific enthalpy of substance m, respectively.

2.2. Turbulence model

This study uses the standard k-ε mode [2], which introduces the turbulent kinetic energy k, and the rate of dissipation of turbulent kinetic energy per unit mass of fluid ε, calculated as follows:

$$\frac{\partial}{\partial t}(\rho k) + \frac{\partial}{\partial x_j}\left(\rho k u_j\right) = -\rho\overline{u_j u_i}\frac{\partial u_i}{\partial x_j} + \frac{\partial}{\partial x_j}\left(\mu + \frac{\mu_t}{\sigma_k}\frac{\partial k}{\partial x_j}\right) - \rho\varepsilon \quad (8)$$

$$\frac{\partial}{\partial t}(\rho\varepsilon) + \frac{\partial}{\partial x_j}\left(\rho\varepsilon u_j\right) = -C_{\varepsilon 1}\rho\overline{u_j u_i}\frac{\partial u_i \varepsilon}{\partial x_j k} + \frac{\partial}{\partial x_j}\left(\mu + \frac{\mu_t}{\sigma_\varepsilon}\frac{\partial k}{\partial x_j}\right) - C_{\varepsilon 2}\rho\frac{\varepsilon^2}{k} \quad (9)$$

$$\mu_t = \rho C_\mu \frac{k^2}{\varepsilon} \quad (10)$$

In the formula, C_μ, $C_{\varepsilon 1}$, $C_{\varepsilon 2}$, σ_k and σ_ε are model constants taking values of 0.09, 1.44, 1.92, 1.0 and 1.3, respectively.

2.3. Combustion model

In this paper, the hydrogen combustion process was simulated using the EDC model [3], this model introduces the Arrhenius chemical reaction kinetics [4-5] while considering the turbulent flow and combines it with the detailed hydrogen combustion reaction mechanism so as to show the details of the combustion process more accurately, and the reaction rate of the species i was calculated according to the following equation:

$$R_m = \frac{\rho(\xi^*)^2}{\tau^*\left[1 - \left(\xi^*\right)^3\right]}\left(Y_m^* - Y_m\right) \quad (11)$$

$$Y_m = (\xi^*)^3 Y_m^* + (\xi^*)^3)Y_m^0 \quad (12)$$

$$\xi^* = C_\xi\left(\frac{\mu\varepsilon}{\rho k^2}\right)^{1/4} \quad (13)$$

$$\tau^* = C_\tau\left(\frac{\mu}{\rho\varepsilon}\right)^{1/2} \quad (14)$$

In the formula, Y_m^* is the mass fraction of species m in the fine structure after reaction at time τ^*; Y_m is the average mass fraction calculated for species m; Y_m^0 denotes the mass fraction of species m in the fluid surrounding the fine structure; ξ^* is the fine-scale length fraction; C_ξ is a volume fraction constant with a value of 2.1377; C_τ is a time-scale constant of 0.4082.

3. Analysis of simulation results

The ambient air humidity will vary depending on the geographical environment, and the simulation in this section sets the ambient temperature as room temperature. This section explores the effect of ambient air humidity changes on the hydrogen jet flame, this subsection were set to air humidity 50 %, 75 %, 100 % of the three sets of parameters, geometric model parameters and boundary settings shown in Figure 1.
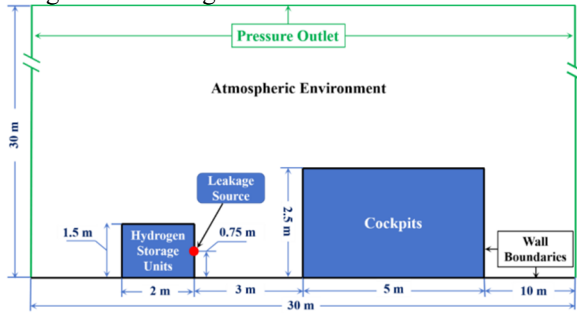

Figure 1. Geometric model

Table 1 shows the mass fraction of each component of the atmosphere at different relative humidities; in the initialization option of the simulation, choose to initialize from the full domain, and enter different parameters in the temperature term so as to change the ambient temperature setting.

Tabler. 1 Mass fraction of atmospheric components under different relative humidity

Relative humidity	Water vapor mass fraction	Oxygen mass fraction	Nitrogen mass fraction
50%	0.0052	0.2189	0.7759
75%	0.0078	0.2183	0.7739
100%	0.0104	0.2177	0.7719

As can be seen in Figure 2, the upper part of the jet flame is shifted towards the cockpit to varying degrees at different ambient air humidities. The range of the jet flame is the smallest at 75 % ambient air humidity, and the range of the jet flame is similar in the cases of 50 % and 100 % ambient air humidity. Overall, there is very little difference in the temperature distribution cloud plots for the three ambient air humidities. Figure 3 illustrates the molar concentration distribution of unburned hydrogen when jet combustion of hydrogen occurs at different air humidities.
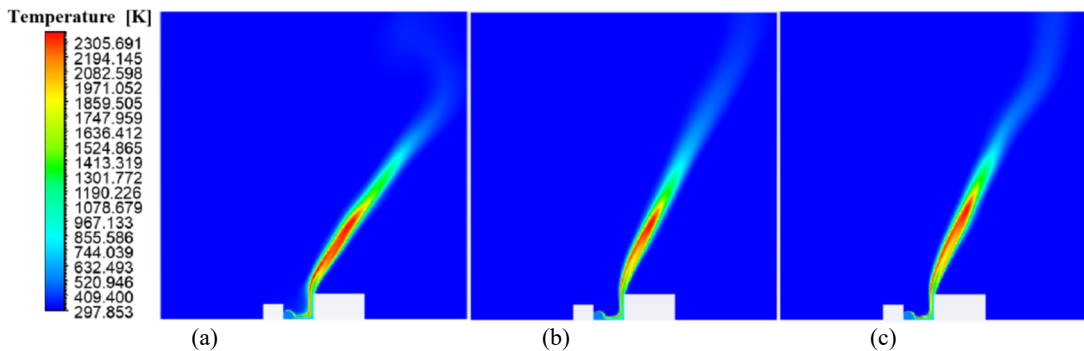

Figure 2. The combustion temperature cloud of hydrogen jet at different ambient air humidity :(a)Air humidity 50 % ; (b) Air humidity 75 % ; (c) Air humidity 100 %
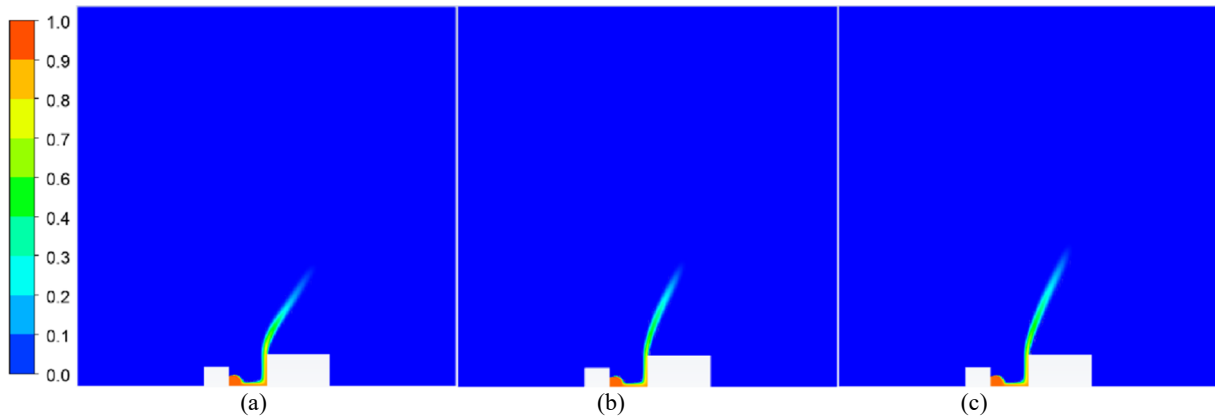

Figure 3. Hydrogen molar concentration cloud diagram at different ambient air humidity:(a)Air humidity 50 % ; (b) Air humidity 75 % ; (c) Air humidity 100 %

Figure 4 shows the distribution curve of hydrogen molar concentration at the cabin height with different ambient air humidity. From the figure, it can be seen that with the increase of ambient air humidity, the distribution of hydrogen molar concentration on the wall surface of the cockpit cabin gradually decreases. The hydrogen molar concentration gradually decreases along the cockpit wall upwards, the hydrogen molar concentration decreases by a similar amount and is relatively smooth, and when it almost reaches the top of the cockpit, a sudden decrease in the hydrogen molar concentration occurs. As shown in Figure 5, as the ambient air humidity rises, the temperature distribution on the cockpit wall decreases gradually, when the ambient air humidity rises from 50 % to 75 %, the overall temperature decreases by about 50 K, and when the ambient air temperature rises from 75 % to

100 %, the overall temperature decreases by about 80 K. The temperature of the jet flame increases gradually and smoothly along the cockpit wall, and when it reaches the top of the cockpit, the temperature of the jet flame decreases by a similar amount and is smooth. At the top of the cockpit, the temperature rises sharply due to the deflection of the jet flame in the direction of the cockpit.
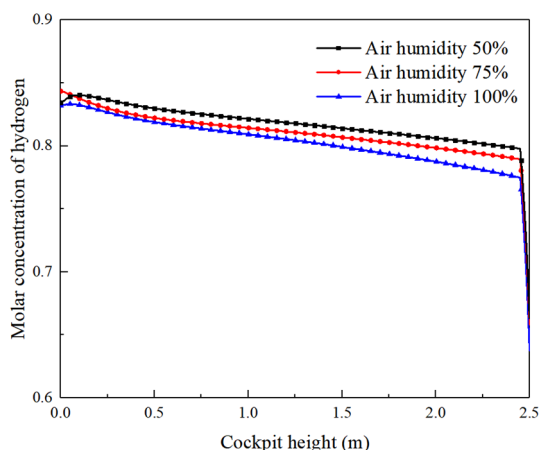

Figure 4. The distribution curve of hydrogen molar concentration at cabin height under different ambient air humidity

Figure 5. Temperature distribution curve of cabin height under different ambient air humidity

Figure 6 shows the distribution curve of hydrogen molar concentration in the jet center axis under different ambient air humidity. It can be concluded from the figure that, under different ambient air humidity, the difference in the distribution of hydrogen molar concentration in the jet center axis is relatively small, and the hydrogen molar concentration in the horizontal distance from the leakage port 0.5-0.8 m and 2.5-2.7 m is slightly different, and there is no obvious law. As shown in Figure 7, within 0.8 m from the horizontal leakage port, the difference in temperature is very small; within 0.8-2.7 m from the horizontal leakage port, with the increase of ambient air humidity, the temperature distributed on the jet center axis gradually decreases; within 2.7-3.0 m from the horizontal leakage port, with the increase of ambient air humidity, the temperature distributed on the jet center axis gradually increases, and the temperature difference is small. and the temperature difference is small. From Figure 8, the maximum negative pressure decreases with the increase

of ambient air humidity, and the pressure is the smallest when the ambient air humidity is 50 % in the positive pressure zone, and the difference of the pressure distribution is small when the ambient air humidity is 75 % and 100 %, and there is no obvious pattern in the positive pressure zone.
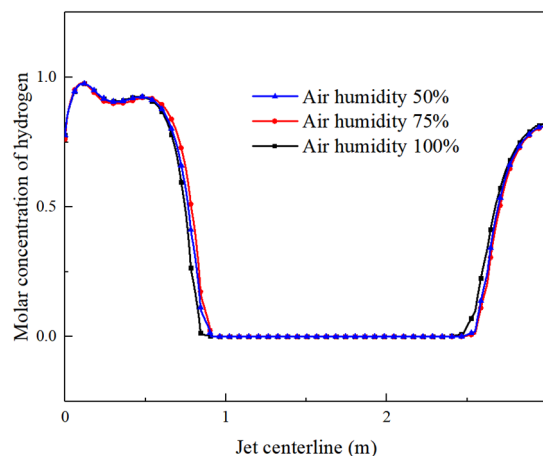

Figure 6. The distribution curve of hydrogen mole concentration in the central axis of the jet at different ambient humidity
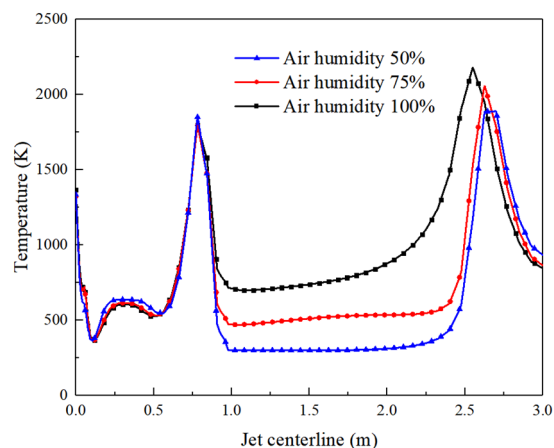

Figure 7 The temperature distribution curve of the central axis of the jet at different ambient humidity
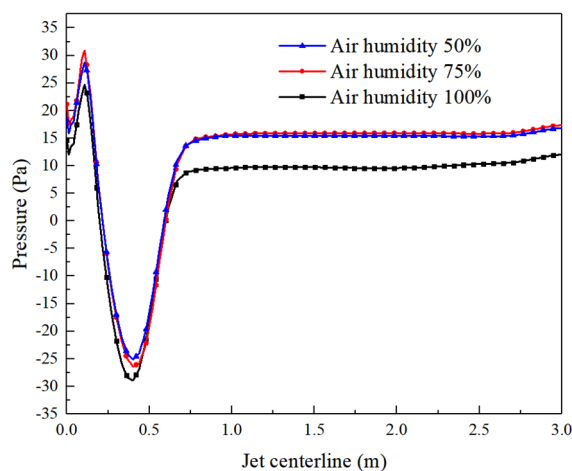

Figure 8 The pressure distribution curve of the central axis of the jet at different ambient humidity

4. Conclusion

Under different ambient air humidity, the upper part of the jet flame was shifted toward the cockpit to different degrees, and the difference in the temperature distribution cloud diagrams under different ambient air humidity was very small. With the increase of ambient air humidity, the molar concentration of hydrogen distributed on the wall surface of the cockpit chamber decreases gradually, and the temperature decreases gradually, and when it reaches the top of the cockpit chamber, the temperature rises abruptly due to the deflection of the jet flame toward the cockpit chamber. The difference in the hydrogen molar concentration distribution in the jet centerline under different ambient air humidity is relatively small; with the increase of ambient air humidity, the difference in temperature is very small within 0.8 m from the horizontal leakage port, the temperature decreases in the range of 0.8-2.7 m from the horizontal leakage port, and the temperature increases in the range of 2.7-3.0 m from the horizontal leakage port and the difference in temperature is relatively small; the max. negative pressure value decreases with the increase of ambient air humidity, and there is no obvious pattern in the positive pressure area.

Acknowledgments

References

1. Shi, J., Zhu, Y., Feng, Y., Yang, J., & Xia, C. (2023). A prompt decarbonization pathway for shipping: Green hydrogen, ammonia, and methanol production and utilization in marine engines. Atmosphere, 14(3), 584.

2. Alam, M., Naser, J., & Brooks, G. (2010). Computational fluid dynamics simulation of supersonic oxygen jet behavior at steelmaking temperature. Metallurgical and Materials Transactions B, 41, 636-645.

3. Giannissi, S. G., Venetsanos, A. G., Bartzis, J. G., Markatos, N., Willoughby, D., Royle, M. (2011). CFD modeling of LH2 dispersion using the ADREA-HF code.

4. Magnussen, B. (1981, January). On the structure of turbulence and a generalized eddy dissipation concept for chemical reaction in turbulent flow. In 19th aerospace sciences meeting (p. 42).

5. Tang, G., Chen, Y., Silaen, A. K., Krotov, Y., Riley, M. F., & Zhou, C. Q. (2019). Investigation on coherent jet potential core length in an electric arc furnace. steel research international, 90(4), 1800381.